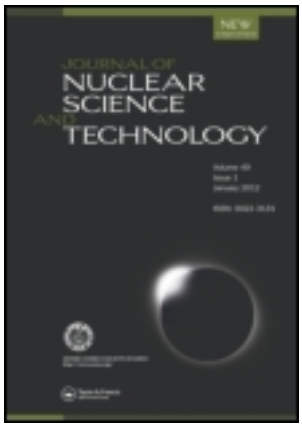

Journal of Nuclear Science and Technology
Publication details, including instructions for authors and subscription information:
http://www.tandfonline.com/loi/tnst20

Simulation of Bubble Motion under Gravity by Lattice Boltzmann Method

Naoki TAKADA [a] , Masaki MISAWA [b] , Akio TOMIYAMA [c] & Shigeo HOSOKAWA [c]

[a] Institute for Environmental Management Technology , AIST, 16-1, Onogawa, Tsukuba-shi , Ibaraki , 305-8569

[b] Institute for Mechanical Systems Engineering , AIST, 1-2, Namiki, Tsukuba-shi , Ibaraki , 305-8564

[c] Graduate School of Science and Technology, Kobe University , 1-1, Rokkodai-cho, Nada-ku , Kobe , 657-8501

Published online: 07 Feb 2012.

To cite this article: Naoki TAKADA , Masaki MISAWA , Akio TOMIYAMA & Shigeo HOSOKAWA (2001) Simulation of Bubble Motion under Gravity by Lattice Boltzmann Method, Journal of Nuclear Science and Technology, 38:5, 330-341, DOI: 10.1080/18811248.2001.9715037

To link to this article: http://dx.doi.org/10.1080/18811248.2001.9715037

Journal of NUCLEAR SCIENCE and TECHNOLOGY, Vol. 38, No. 5, p. 330–341 (May 2001)

Simulation of Bubble Motion under Gravity by Lattice Boltzmann Method

Naoki TAKADA[1,*], Masaki MISAWA[2], Akio TOMIYAMA[3] and Shigeo HOSOKAWA[3]

[1]*Institute for Environmental Management Technology, AIST, 16-1, Onogawa, Tsukuba-shi, Ibaraki, 305-8569*
[2]*Institute for Mechanical Systems Engineering, AIST, 1-2, Namiki, Tsukuba-shi, Ibaraki, 305-8564*
[3]*Graduate School of Science and Technology, Kobe University, 1-1, Rokkodai-cho, Nada-ku, Kobe 657-8501*

(Received March 29, 2000)

We describe the numerical simulation results of bubble motion under gravity by the lattice Boltzmann method(LBM), which assumes that a fluid consists of mesoscopic fluid particles repeating collision and translation and a multiphase interface is reproduced in a self-organizing way by repulsive interaction between different kinds of particles. The purposes in this study are to examine the applicability of LBM to the numerical analysis of bubble motions, and to develop a three-dimensional version of the binary fluid model that introduces a free energy function. We included the buoyancy terms due to the density difference in the lattice Boltzmann equations, and simulated single- and two-bubble motions, setting flow conditions according to the Eötvös and Morton numbers. The two-dimensional results by LBM agree with those by the Volume of Fluid method based on the Navier-Stokes equations. The three-dimensional model possesses the surface tension satisfying the Laplace's law, and reproduces the motion of single bubble and the two-bubble interaction of their approach and coalescence in circular tube. These results prove that the buoyancy terms and the 3D model proposed here are suitable, and that LBM is useful for the numerical analysis of bubble motion under gravity.

KEYWORDS: lattice Boltzmann method, numerical simulation, numerical analysis, binary fluid model, two-phase fluid, volume of fluid method, bubbles, surface tension, Laplace's law, buoyancy, bubble coalescence

I. Introduction

The lattice Boltzmann method (LBM)[1)] has been proposed as a mesoscopic approach to the numerical simulations of fluid motions on the statistical-thermodynamic assumption that a fluid consists of many virtual particles repeating collision and translation through which their velocity distributions converge to a state of local equilibrium. Lattice Boltzmann method, based on the lattice gas cellular automaton,[2,3)] possesses the advantages such as relatively easy implementation of boundary conditions on complicated geometry, high efficiency on parallel processing, and flexible reproduction of interface between multiple phases. The last point on which we focus in this study arises from the introduction of repulsive interaction between particles without any boundary condition for interface. As a result, LBM is more useful than other conventional methods for the numerical analysis of multiphase fluid system, where the flow pattern changes not only spatially but also temporally due to deformation, break up, and coalescence of droplet or bubble. That is the reason why we apply LBM to the simulations of two-phase fluid motion. The low- and high-density fluids in this study, referred to as bubble and liquid respectively, correspond to the pressurized fluids having a small density ratio such as steam and water in PWR nuclear power plants. Another advantage of LBM occurs on implementation of complicated boundary conditions to be seen in fuel assemblies, although the topic is not discussed in detail in this study. Lattice Boltzmann method therefore is a promising method suitable for simulating fluid flows in nuclear engineering.

In single-phase LBM, there have already been a lot of numerical results for incompressible viscous fluid flows.[4–7)] On the other hand, several kinds of multiphase fluid model have recently been proposed and applied to the simulations of phase separation and transition. The first immiscible multiphase model[8,9)] reproduced the phase separation by the repulsive interaction based on the color gradient and the color momentum between red- and blue-colored particles representing two kinds of fluid. Shan and Chen proposed the gas-liquid model applicable to the phase transition with the potential between particles,[10,11)] while another gas-liquid model proposed by Swift *et al.*[12)] simulates phase transitions consistent with the thermodynamics on the theory of van der Waals-Cahn-Hillard free energy. Kato *et al.* also presented a two-phase model with a pseudo potential for van der Waals fluids.[13)] Lattice Boltzmann method was used to simulate the condensation of liquid droplets in supersaturated vapor, the two-phase fluid flow through sandstone in three dimensions and so on.[14,15)] However, it has not been applied to any quantitative numerical analysis of the motion of bubble or droplet in two-phase flows under gravity in two and three dimensions, because the main purpose in previous works was to develop multiphase model and examine its property, or to reproduce fundamental phenomena in multiphase fluid where buoyancy effect is negligible.

Therefore, in LBM, we consider the buoyancy effect due to density difference in two-phase fluid characterized with the non-dimensional numbers such as Eötvös and Morton numbers, and develop the three-dimensional version of the binary fluid model which is a newest one proposed by Swift

*Corresponding author, Tel. +81-298-61-8232,
Fax. +81-298-61-8722,
E-mail: naoki-takada@aist.go.jp or naoki_takada@hotmail.com

et al.[16,17] This model using the free-energy approach has one important improvement that the equilibrium distribution of fluid particles can be defined consistently based on thermodynamics, compared with other models which are based on phenomenological models of interface dynamics. Consequently, the total energy, including the surface energy, kinetic energy, and internal energy can be conserved.[18] Furthermore, it also reproduces Galilean invariance more properly than one-component fluid model.[16] In this paper, we show the numerical results of bubble motions, which are compared with the two-dimensional results by the Volume of Fluid (VOF) method based on the finite difference of macroscopic hydrodynamic equations.[19] The three-dimensional results by LBM are also presented for the coalescence of bubbles.

First, we explain LBM and the binary fluid model in the next chapter, and the three-dimensional version in Chap. III. After the buoyancy terms and the non-dimensional numbers in LBM are described in Chap. IV, the numerical results will be presented in Chap. V. The conclusion in this study is described in the last chapter.

II. Basis of Lattice Boltzmann Binary Fluid Model

This chapter describes a basis of the lattice Boltzmann method and the binary fluid model. The typical LBM discretizes a space uniformly to be isotropic, with hexagonal or square lattice in two dimensions,[3,4,16] and with cubic lattice in three dimensions.[20] On such a discrete space, a macroscopic fluid is replaced with the population of mesoscopic fluid particle with unit mass, which possesses real-valued number densities and is allowed to be rest at lattice sites or to move with constant velocity set along lattice lines. They repeat two kinds of motion during one time step all over the space; translation from site to site, and elastic collision with each other at each lattice site. The collision is operated statistically according to the rule to conserve mass and momentum of particles, which corresponds to a relaxation process that the distributions of particles approach to a state of local equilibrium. As a result, a macroscopic fluid dynamics in LBM appears emergently from averaging particle motions.

In modeling two-phase fluid, we use the binary fluid model proposed by Swift *et al.*,[16] called BFSY model here. A binary fluid consists of two kinds of particle population with number densities n_A and n_B, which represent two fluid components A and B respectively. The repulsive interaction is associated with a free energy function, and introduced only between A and B particles, which causes two-phase separation into an A-rich and B-rich regions below a given critical temperature. In the BFSY model, there are two independent macroscopic densities, total number density of two fluid components, $n = n_A + n_B$, and number density difference between A and B, $\Delta n = n_A - n_B$. The total density n is proportional to pressure and approximately constant in the whole flow field, while the function Δn becomes positive in the region where $n_A > n_B$ and negative in the other one and then represents two-phase distribution. These densities are equivalent to the summations of the distribution functions of particle number densities, f_a and g_a, respectively as follows,

$$n = \sum_a f_a, \tag{1}$$

$$\Delta n = \sum_a g_a. \tag{2}$$

The index a denotes a label to distinguish particles by their velocity. A flow velocity $\boldsymbol{u}$ is also defined by the following,

$$n\boldsymbol{u} = \sum_a f_a \boldsymbol{e}_a, \tag{3}$$

where $\boldsymbol{e}_a$ is the velocity vector of particles moving from a lattice site at position $\boldsymbol{r}$ to its neighbor at $\boldsymbol{r}+\boldsymbol{e}_a\Delta t$ during one time increment Δt, and $|\boldsymbol{u}| \ll |\boldsymbol{e}_a|$ because the LBM application is limited within low Mach number.

The evolution of distribution functions are governed by two kinds of the lattice Boltzmann equations with the lattice BGK (Bhatnagar-Gross-Krook) collision operators,[21]

$$f_a(t+\Delta t, \boldsymbol{r}+\boldsymbol{e}_a\Delta t) = f_a(t,\boldsymbol{r}) - \frac{1}{\tau_1}\left[f_a(t,\boldsymbol{r}) - f_a^{eq}(t,\boldsymbol{r})\right], \tag{4}$$

$$g_a(t+\Delta t, \boldsymbol{r}+\boldsymbol{e}_a\Delta t) = g_a(t,\boldsymbol{r}) - \frac{1}{\tau_2}\left[g_a(t,\boldsymbol{r}) - g_a^{eq}(t,\boldsymbol{r})\right], \tag{5}$$

where t is the time, τ_1 and τ_2 are the relaxation time parameters, related with macroscopic transport coefficients, and the superscript eq denotes a local equilibrium state. In the two-dimensional hexagonal lattice with link length=1,[2,16] the subscript a corresponds to the index i of the direction along link lines, $i = 1$ to 6 for moving particles with constant speed $c=1/\Delta t$ and $i=0$ for stationary particles. On the other hand, in the three-dimensional lattice consisting of two kinds of the link lines with their length unity and $\sqrt{3}$,[20] it is replaced with two indices l and i to specify the kind of link lines and the direction respectively, as described in Chap. III. The above Eqs. (4) and (5) indicate that the distributions reach the states of local equilibrium f_a^{eq} and g_a^{eq} after time periods $\tau_1\Delta t$ and $\tau_2\Delta t$. This relaxation process requires the parameters τ_1 and τ_2 larger than 0.5, which mean that the collision operators include eigenvalues over -2.0. If they are lower than 0.5, LBM simulation is always unstable because the distribution functions do not approach to equilibrium values through collision process.

The macroscopic variables, n, Δn, and momentum $n\boldsymbol{u}$ can be conserved locally at each lattice site in the collision, because the equilibrium distributions satisfy following relations,

$$n = \sum_a f_a^{eq}, \tag{6}$$

$$\Delta n = \sum_a g_a^{eq}, \tag{7}$$

$$n\boldsymbol{u} = \sum_a f_a^{eq}\boldsymbol{e}_a. \tag{8}$$

In addition, g_a^{eq} also satisfies the following relation,

$$\Delta n\boldsymbol{u} = \sum_a g_a^{eq}\boldsymbol{e}_a. \tag{9}$$

In order to describe the thermodynamic behavior of binary fluid appropriately, the BFSY model incorporates the free energy function Ψ which defines an equilibrium state in two-phase coexistence by its minimum value,[16]

$$\Psi = \int \left[\psi + \frac{\kappa}{2}(\nabla n)^2 + \frac{\kappa}{2}(\nabla \Delta n)^2\right] d\boldsymbol{r}, \tag{10}$$

where ψ is the bulk free energy density and κ is a control parameter of surface tension. The function Ψ causes circular-symmetry pressure tensor $P_{\alpha\beta}$ and chemical potential difference $\Delta\mu$,

$$P_{\alpha\beta} = p\delta_{\alpha\beta} + \kappa\left(\frac{\partial n}{\partial r_\alpha}\cdot\frac{\partial n}{\partial r_\beta} + \frac{\partial \Delta n}{\partial r_\alpha}\cdot\frac{\partial \Delta n}{\partial r_\beta}\right), \tag{11}$$

$$\Delta\mu = \frac{\delta\Psi}{\delta(\Delta n)} = -\frac{\lambda}{2}\cdot\frac{\Delta n}{n} + \frac{T}{2}\ln\left(\frac{n+\Delta n}{n-\Delta n}\right) - \kappa\nabla^2(\Delta n), \tag{12}$$

where the Greek subscripts are Cartesian coordinate indices, $\delta_{\alpha\beta}$ the sign of Kronecker's delta, and

$$\begin{aligned} p &= \Delta n\frac{\delta\Psi}{\delta(\Delta n)} + n\frac{\delta\Psi}{\delta n} - \Psi \\ &= nT - \kappa\left[n\nabla^2 n + \Delta n\nabla^2(\Delta n)\right] \\ &\quad - \frac{\kappa}{2}\left(|\nabla n|^2 + |\nabla\Delta n|^2\right). \end{aligned} \tag{13}$$

In the above equations, λ represents the strength of interaction, T is the temperature of fluid. As a result, two-phase separation is caused when T, a constant for whole flow field, is lower than the critical temperature $T_c = \lambda/2$. In the BFSY model, Eqs. (11) and (12) are obtained from summing higher velocity moments of f_a^{eq} and g_a^{eq} respectively,

$$P_{\alpha\beta} = \sum_a f_a^{eq}(\boldsymbol{e}_{a\alpha} - u_\alpha)\left(\boldsymbol{e}_{a\beta} - u_\beta\right), \tag{14}$$

$$\Gamma\Delta\mu\delta_{\alpha\beta} = \sum_a g_a^{eq}(e_{a\alpha} - u_\alpha)\left(e_{a\beta} - u_\beta\right), \tag{15}$$

where the parameter Γ represents the mobility.

The macroscopic dynamics of binary fluid in LBM can be derived from the mesoscopic evolution equations (4) and (5) through the multi-scale expansion technique.[3,16] The former equation is related with the continuum equation and the equation of fluid motion, while the latter leads to the convection-diffusion equation for the function Δn corresponding to the two-phase distribution. First, by Taylor-expansion in Eq. (4) around $(t, \boldsymbol{r})$ up to second order, the following equation is obtained,

$$\begin{aligned} &\frac{\partial f_a}{\partial t} + e_{a\alpha}\frac{\partial f_a}{\partial r_\alpha} + \frac{1}{2}\cdot\frac{\partial^2 f_a}{\partial t^2}\Delta t + e_{a\alpha}\frac{\partial^2 f_a}{\partial t\partial r_\alpha}\Delta t \\ &\quad + \frac{1}{2}e_{a\alpha}e_{a\beta}\frac{\partial^2 f_a}{\partial r_\alpha\partial r_\beta}\Delta t = -\frac{1}{\Delta t\tau_1}\left(f_a - f_a^{eq}\right), \end{aligned} \tag{16}$$

where the repeat of α and β denotes the convention of summation. The distribution function f_a can also be expanded around a state of local equilibrium f_a^{eq}, assuming that the deviation from equilibrium ${f_a}^{neq}$ is slight,

$$f_a = f_a^{eq} + {f_a}^{neq} = f_a^{eq} + \epsilon f_a^{(1)} + \epsilon^2 f_a^{(2)} + \dots, \tag{17}$$

where ϵ is a small parameter corresponding to the Knudsen number, and the non-equilibrium distribution components $f_a^{(l)}(l = 1, 2, \dots)$ obviously satisfy the following equations,

$$\sum_a f_a^{(l)} = 0, \tag{18}$$

$$\sum_a f_a^{(l)}\boldsymbol{e}_a = \boldsymbol{0}. \tag{19}$$

On the other hand, the mesoscopic time and spatial scales in Eq. (16), t and r_α, are changed into the macroscopic ones, using ϵ as follows:

$$\frac{\partial}{\partial t} = \epsilon\frac{\partial}{\partial t_1} + \epsilon^2\frac{\partial}{\partial t_2}, \tag{20}$$

$$\frac{\partial}{\partial r_\alpha} = \epsilon\frac{\partial}{\partial r_{1\alpha}}. \tag{21}$$

The first order of ϵ denotes the scale in a flow system governed by the Euler equations, and the second order is required in order to observe diffusive phenomena.

Substituting Eqs. (17), (20), and (21) into Eq. (16) and taking the terms up to second order of ϵ lead to the following equation,

$$\begin{aligned} &\left(\frac{\partial}{\partial t_1} + \frac{\partial}{\partial t_2}\right) f_a^{eq} + e_{a\alpha}\frac{\partial f_a^{eq}}{\partial r_{1\alpha}} + \left(1 - \frac{1}{2\tau_1}\right) \\ &\quad \times\left[\frac{\partial f_a^{(1)}}{\partial t_1} + e_{a\alpha}\frac{\partial f_a^{(1)}}{\partial r_{1\alpha}}\right] = -\frac{1}{\Delta t\tau_1}\left(f_a^{(1)} + f_a^{(2)}\right). \end{aligned} \tag{22}$$

Finally, the conservation equations of mass and momentum of fluid are derived from summing all the zero-th and first-order velocity moments $\boldsymbol{e}_a$ of Eq. (22) respectively under the conditions, Eqs. (20), (21), and the relation in first order of ϵ,

$$\frac{\partial f_a^{eq}}{\partial t_1} + e_{a\alpha}\frac{\partial f_a^{eq}}{\partial r_{1\alpha}} = -\frac{1}{\Delta t\tau_1}f_a^{(1)}. \tag{23}$$

The macroscopic equations in LBM correspond to the Navier-Stokes ones when the equilibrium distribution satisfies Eqs. (6), (8), and (14).

The same arithmetic way is applied to Eq. (5) to derive the macroscopic equation governing phase convection-diffusion phenomena under the conditions, Eqs. (7), (9), and (15),

$$\begin{aligned} \frac{\partial\Delta n}{\partial t} + \frac{\partial\Delta n u_\alpha}{\partial r_\alpha} &= \left(\tau_2 - \frac{1}{2}\right) \\ &\quad \times\Delta t\frac{\partial}{\partial r_\alpha}\left[\Gamma\frac{\partial\Delta\mu}{\partial r_\alpha} - \frac{\Delta n}{n}\cdot\frac{\partial P_{\alpha\beta}}{\partial r_\beta}\right]. \end{aligned} \tag{24}$$

The right hand side of Eq. (24) reduces into zero in a state of equilibrium because of constant $\Delta\mu$ and pressure balance,[17]

$$\frac{\partial P_{\alpha\beta}}{\partial r_\beta} = 0. \tag{25}$$

III. Three-dimensional Binary Fluid Model

We developed the three-dimensional version based on the two-dimensional BFSY model.[16] In the isotropic discretization of space and particle velocity, this model uses the same

cubic lattice unit as the 15-velocity model(3D15V model) proposed by Chen *et al.*[20] The subscript a in the distribution functions is replaced with two indices, l and i. The former index l is the identification index of two kinds of the lattice links with their length unity and $\sqrt{3}$, while the latter i is the index of the direction along lattice lines, $i = 1$ to 6 for $l = 1$, $i = 1$ to 8 for $l = 2$. $l = 0$ is assigned to stationary particles. The equilibrium distributions $f_{l,i}^{eq}$ are represented on the limit of low Mach number by,

$$f_{l,i}^{eq} = n\left[A_l + B_l\frac{(\boldsymbol{e}_{l,i}\cdot\boldsymbol{u})}{c^2} + C_l\frac{(\boldsymbol{e}_{l,i}\cdot\boldsymbol{u})^2}{c^4} + D_l\frac{(\boldsymbol{u}\cdot\boldsymbol{u})}{c^2}\right] + G_{\alpha\beta}^{(l)}e_{l,i,\alpha}e_{l,i,\beta}, \tag{26}$$

$$f_0^{eq} = n\left[A_0 + D_0\frac{(\boldsymbol{u}\cdot\boldsymbol{u})}{c^2}\right], \tag{27}$$

where $c\Delta t = 1$, and the particles moves with the speeds $2c$ and $\sqrt{3}c$ on two link lines $l = 1$ and 2 respectively.

The dimensionless parameters A_l, B_l, C_l, and D_l are determined under the constraints to derive the Navier-Stokes equations from Eq. (4) in the way described in Chap. II. As for A_l ($l = 0, 1, 2$), the following equations are given,

$$A_l = \frac{s_l}{8(s_1+s_2)c^2}\left[T - \kappa\left(\frac{\Delta n}{n}\nabla^2\Delta n + \nabla^2 n\right)\right], \tag{28}$$

$$A_0 = 1 - 6A_1 - 8A_2, \tag{29}$$

where $s_l (l = 0, 1, 2)$ denotes the ratio of number density of particles in stationary equilibrium state, satisfying $s_0 + 6s_1 + 8s_2 = 1$, which determines the temperature T,

$$T = 8(s_1+s_2)c^2. \tag{30}$$

The fluid in 3D15V model possesses the kinetic viscosity ν,

$$\nu = 4B_2\,(2\tau_1 - 1)\,c^2\Delta t. \tag{31}$$

The derivation of the Navier-Stokes equations from Eq. (4) requires that the parameters in Eqs. (26) and (27) satisfy the following algebraic relations,

$$B_1 + B_2 = \frac{1}{8}, \tag{32}$$

$$8C_1 + 6D_1 + 8C_2 + 8D_2 + D_0 = 0, \tag{33}$$

$$C_2 = \frac{1}{16}, \tag{34}$$

$$4C_1 - C_2 + D_1 + D_2 = 0. \tag{35}$$

The first and second relations arise from Eq. (6), while the others, Eqs. (34) and (35), are derivable from Eq. (14). In this study, B_1 and B_2 are either 1/24 or 1/12 respectively, and the other parameters are determined as follows:

$$C_1 = \frac{1}{32}, \quad D_0 = -\frac{7}{24}, \quad D_1 = -\frac{1}{48}, \quad D_2 = -\frac{1}{24}.$$

The tensor $G_{\alpha\beta}^{(l)}$ in Eq. (26) which yields the surface tension is defined as,

$$G_{\alpha\beta}^{(l)} = \frac{\kappa}{c^4}\left[E_l\left(\frac{\partial n}{\partial r_\alpha}\cdot\frac{\partial n}{\partial r_\beta} + \frac{\partial\Delta n}{\partial r_\alpha}\cdot\frac{\partial\Delta n}{\partial r_\beta}\right) + F_l\left(|\nabla n|^2 + |\nabla\Delta n|^2\right)\delta_{\alpha\beta}\right]. \tag{36}$$

E_l and F_l are the parameters determined by two constraints of the mass conservation in collision process (Eq. (6)) and the derivation of the pressure tensor $P_{\alpha\beta}$ (Eq. (11)) from Eq. (14),

$$\sum_{l,i} G_{\alpha\beta}{}^{(l)}e_{l,i,\alpha}e_{l,i,\beta} = 0, \tag{37}$$

$$\sum_{l,i}\left(nA_l + G_{\gamma\delta}{}^{(l)}e_{l,i,\gamma}e_{l,i,\delta}\right)e_{l,i,\alpha}e_{l,i,\beta} = P_{\alpha\beta}. \tag{38}$$

Calculating the summation of even-order particle velocity moments on the spatial isotropy,[20] the following results can be obtained,

$$E_1 = F_1 = \frac{1}{32}, \quad E_2 = -\frac{1}{16}, \quad F_2 = 0. \tag{39}$$

The equilibrium distribution functions in the binary fluid model, Eq. (26), correspond to those in the single phase fluid model[20] exactly when the gradients of n and Δn vanish.

The another equilibrium distributions for Δn, $g_{l,i}^{eq}$, are computed according to the following equations:

$$g_{l,i}^{eq} = B_l\frac{\Gamma\Delta\mu}{c^2} + \Delta n\left[B_l\frac{(\boldsymbol{e}_{l,i}\cdot\boldsymbol{u})}{c^2} + C_l\frac{(\boldsymbol{e}_{l,i}\cdot\boldsymbol{u})^2}{c^4} + D_l\frac{(\boldsymbol{u}\cdot\boldsymbol{u})}{c^2}\right], \tag{40}$$

$$g_0^{eq} = \Delta n - \frac{\Gamma\Delta\mu}{c^2}\left(\sum_{l,i} B_l\right) + \Delta n D_0\frac{(\boldsymbol{u}\cdot\boldsymbol{u})}{c^2}. \tag{41}$$

Because of $\sum_a \left(g_a - g_a^{eq}\right)\boldsymbol{e}_a \neq \boldsymbol{0}$, the evolution equation in the BFSY model (5) includes the macroscopic diffusive effect of density difference function Δn, even though it is conserved locally at each lattice site in the collision step. In this study, we adjust Γ to suitable values through test runs in order to retain the initial volume of gas phase in simulating two-phase fluid motions without diffusion. As far as we know, there has been no description how to set Γ consistently in previous works.[16,17] Therefore, the test run is the only useful process now although it requires extra computation time. The scheme to determine the mobility parameter is still under consideration, not only for the two-phase fluid without phase transition, but also for the unsteady state in boiling and condensation.

IV. Buoyancy Effect in Binary Fluid Model

In this study, we introduced the buoyancy terms δf_a and δg_a to the lattice Boltzmann equations (4) and (5) in order to consider the effect due to the density difference between liquid and gas phases. Hereafter, for the sake of convenience, a low-density and high-density phases, having the densities n_L and n_G, are referred to as gas and liquid respectively. Assumed that the liquid and gas phases correspond to the fluids in an A-rich and B-rich regions respectively, n and Δn can be redefined by the following equations,

$$n = \frac{n_L + n_G}{2}, \tag{42}$$

$$\Delta n = n_L F + n_G (1 - F) - n, \tag{43}$$

where $0<F<1$ is the volume ratio of liquid phase. The function Δn takes the same absolute value Δn_0 in the liquid ($F = 1$) and the gas ($F = 0$) phases,

$$\Delta n_0 = \frac{n_L - n_G}{2}. \tag{44}$$

The buoyancy terms are available only in the low density phase where the function Δn is negative, and satisfies the constraints of the net varieties of total number density and total momentum of particles as follows:

$$\sum_a \delta f_a = 0, \tag{45}$$

$$\sum_a \delta f_a \boldsymbol{e}_a = -\Delta n^* \boldsymbol{g} \Delta t, \tag{46}$$

where $\Delta n^* = 2\Delta n_0 = n_L - n_G$ is density difference between liquid and gas phases.

The effect of buoyancy increases the number density distributions f_a in the opposite direction to the gravity $\boldsymbol{g}$ according to its magnitude $|\boldsymbol{g}|$ and Δn^*, decreasing those in the gravity direction. On the other hand, the number density difference distributions g_a in the gravity direction increase, because the gas phase corresponds to the negative region of Δn. Then, the following relation is satisfied,

$$\delta g_a = -\delta f_a. \tag{47}$$

In two dimensions, the buoyancy term δf_i is added in the right hand side of Eq. (4) for the moving particles,[22]

$$\delta f_i = \frac{\Delta n^*}{4} \cdot \frac{e_{i,y}}{|e_{i,y}|} \cdot \frac{|\boldsymbol{g}|\Delta t}{c} \quad (i = 1, \ldots, 6), \tag{48}$$

where $e_{i,y}$ is the y-direction component of particle velocity in i-th direction (see **Fig. 1**). In three dimensions, we use the following equation (49) to determine the buoyancy terms in the 15 directions of particle velocity simply,

$$\delta f_{l,i} = -\frac{s_l \Delta n^* \left(\boldsymbol{g} \cdot \boldsymbol{e}_{l,i}\right)}{8(s_1 + s_2)c^2}, \tag{49}$$

with $f_{l,i}^{eq}$ excluding the gradient terms of n and Δn. The expression of the three-dimensional buoyancy term is different from the two-dimensional one, but both of the terms are quite equivalent in the macroscopic effect because they satisfy Eqs. (45) and (46).

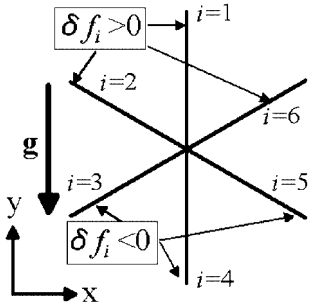

Fig. 1 The buoyancy terms δf_i in case of hexagonal lattice

The verification of non-dimensional numbers in LBM, that is, Eötvös and Morton numbers, E_o and M, are necessary to apply LBM to the two-phase flow analysis. In general, these numbers are defined with liquid viscosity ν_L, gas and liquid densities, ρ_G and ρ_L, surface tension σ, and characteristic length d as follows:

$$E_o = \frac{|\boldsymbol{g}| (\rho_L - \rho_G) d^2}{\sigma}, \tag{50}$$

$$M = \frac{|\boldsymbol{g}| \rho_L^2 \nu_L^4 (\rho_L - \rho_G)}{\sigma^3}. \tag{51}$$

In LBM, the surface tension σ is not given as a known macroscopic parameter, but results from the mesoscopic interaction between two kinds of fluid particles. Then, we determine the surface tension according to the Laplace's law, which describes the balance of forces due to pressure difference and surface tension on interface. In two dimensions, it is represented by the equation,

$$\sigma = (P_{in} - P_{out}) R, \tag{52}$$

where R is a curvature radius of interface, and P_{in} and P_{out} indicate the pressures inside and outside the gas phase fluid. Considering the buoyancy force according to Eq. (46), E_o and M in the BFSY model are defined as follows:

$$E_o = \frac{2|\boldsymbol{g}|\Delta n^* d_B}{(P_{in} - P_{out})}, \tag{53}$$

$$M = \frac{8|\boldsymbol{g}|\Delta n^* {n_L}^2}{{d_B}^3 (P_{in} - P_{out})^3} \left(\frac{2\tau_1 - 1}{8} \Delta t c^2\right)^4. \tag{54}$$

In Eq. (53), the characteristic length d corresponds to bubble diameter $d_B = 2R$. Setting E_o and M in the simulations, we use the value of σ working on the interface in stationary fluid without gravity.

V. Numerical Results of Bubble Motions

We simulated two- and three-dimensional two-phase fluid motions under gravity, using the 3D BFSY model and the buoyancy terms mentioned in the above sections. Both of 2D and 3D simulations are carried out with the boundary conditions for stationary or moving solid wall, uniform inflow, and free outflow, in which the distribution functions f_a and g_a are reset to local equilibrium states f_a^{eq} and g_a^{eq} at every time step after collision and translation operations.[4,6] The traditional lattice Boltzmann equation (4) intends to be unstable in low-viscous fluid flow (*i.e.* low Morton number) because the Courant number is equal to 1 in 2D and 2 in 3D.[23] In addition, it also gives rise to numerical instability in high density ratio. Therefore, we chose two-phase fluid with high viscosity and low density ratio in the first step of LBM simulation of bubble motion under gravity. The numerical stability in LBM can be improved by other finite difference schemes.[13,23]

1. Two-dimensional Results in LBM and Volume of Fluid Method

Here, the two-dimensional simulations of bubble motion are shown in comparison with those by the VOF method,[19] which is one of the volume tracking method. The VOF method can simulate two-phase fluid motions by solving the

Table 1 The parameters in the simulation of single bubble

Case	E_o	M	$\|\mathbf{g}\|$
(a)	5	0.2267	7.750E-5
(b)	10	0.4535	1.550E-4
(c)	20	0.9070	3.100E-4
(d)	40	1.8134	6.200E-4
(e)	100	4.5350	1.550E-3

Navier-Stokes equations and the convection equation for the volume ratio of liquid phase F,

$$\frac{\partial F}{\partial t} + \nabla \cdot (F\boldsymbol{u}) = 0. \tag{55}$$

In LBM, Eq. (55) is derived from substituting Eq. (43) into Eq. (24) when the macroscopic diffusion is negligible by adjusting the mobility Γ.

First of all, we simulated the two-dimensional single bubble motions in the stationary fluid. The density difference Δn^* is 0.84 for n_L=1.42 and n_G=0.58, corresponding to n=1, κ=0.02, d_B=20, λ=1.1, and T=0.5, which result in σ=0.00521, the relaxation time parameters τ_1=τ_2=1, and Γ=0.05. The flow field is surrounded with stationary walls, and initially a circular-shaped bubble is located in the lower region. This simulation was implemented with 80 lattice sites in x-direction and 300 in y-direction along the buoyancy force under several conditions of E_o and M, as shown in **Table 1**. The magnitude of gravity $|\boldsymbol{g}|$ was determined from the definition of E_o described in Eq. (53). The five figures in **Fig. 2** show the flow velocity fields and the bubble shapes, simulated with LBM and VOF method. For each case, the bubbles are rising at constant velocities because of the balance between buoyancy and drag forces. For example, as shown in **Figs. 3**(a) and (b), the bubble velocities in Case (b) and Case (d) have reached constant values after about 2,000 and 1,000 time steps respectively, in both of LBM and VOF method simulations. In Fig. 2, the interface indicates the position where the density difference function Δn becomes zero. In terms of the shapes of bubble and the wake, the results obtained by LBM are similar to those by VOF method qualitatively, except the degree of deformation. As for the terminal velocity of bubble V_t, good agreement was obtained between LBM and VOF results within several percent error, as shown in **Fig. 4** and **Table 2**. We are now considering why the degree of bubble deformation in LBM is different from that in the VOF method.

In the second place, the numerical results of bubble motion in uniform shear flow are presented for two cases, (a) E_o=10 and M=0.82, (b) E_o=1 and M=0.089, where the right side wall of a duct is moving upward at constant speed $4V_t$. The ratio of bubble diameter d_B=12 to the duct width is about 0.25 in both cases. Initially, the circular bubble is located near the left stationary wall in Case (a), while the location in Case (b) is the center of duct. **Figure 5** shows that the bubbles slide to the center of duct as rising for Case (a) and rise up straightly for Case (b) in both results by LBM and VOF method. Also, the flow velocity and the bubble shape

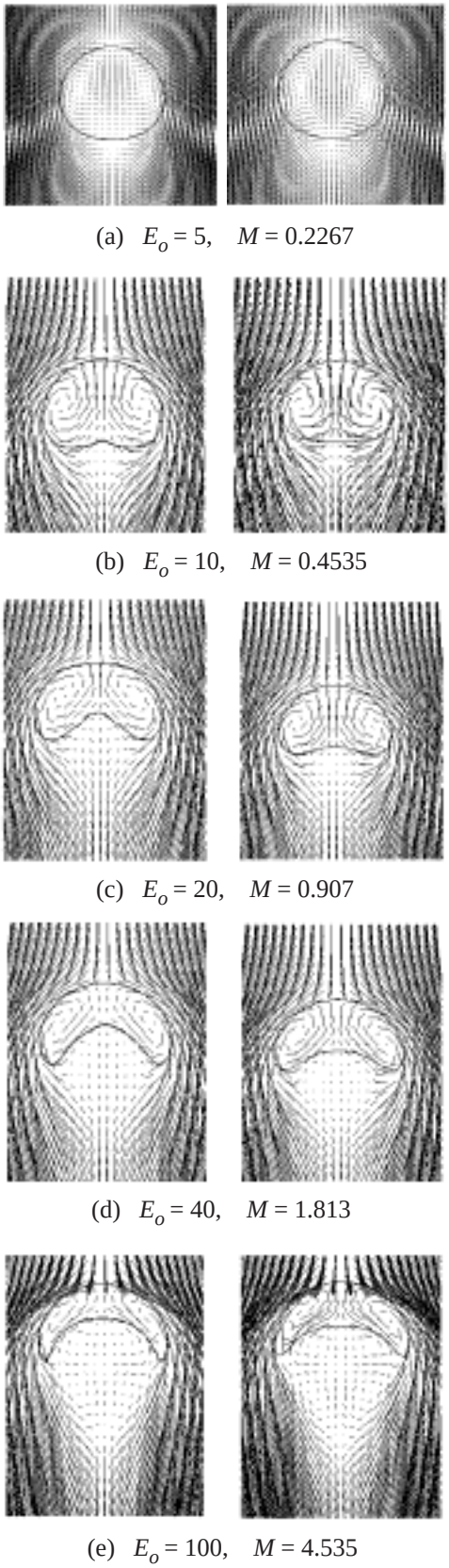

(a) E_o = 5, M = 0.2267

(b) E_o = 10, M = 0.4535

(c) E_o = 20, M = 0.907

(d) E_o = 40, M = 1.813

(e) E_o = 100, M = 4.535

Fig. 2 The two-dimensional flow velocities and interfacial profiles of rising bubble simulated with LBM (left) and VOF method (right)

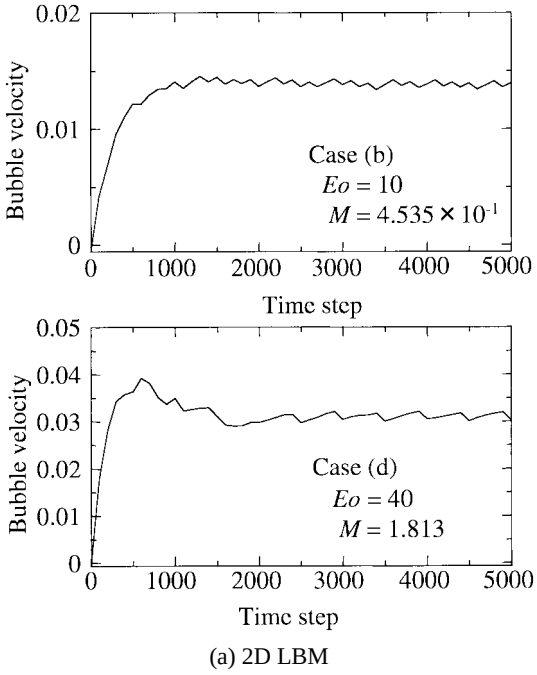

(a) 2D LBM

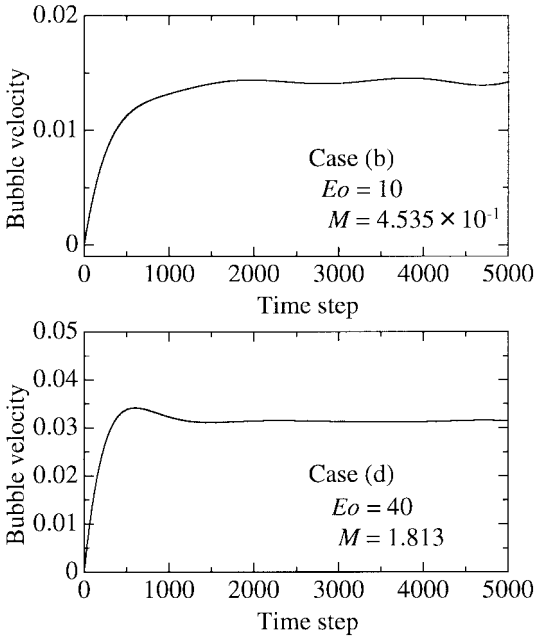

(b) VOF method

Fig. 3 The bubble velocities simulated with (a) 2D LBM and (b) VOF method in Case (b) and Case (d)

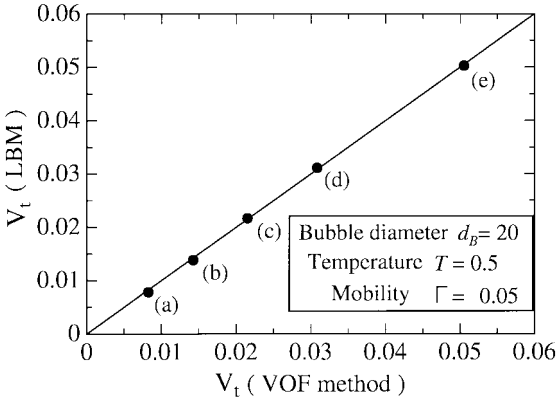

Fig. 4 The terminal rising velocities of bubble in LBM and VOF method simulations

Table 2 The terminal velocity of single bubble V_t

Case	V_t(LBM)	V_t(VOF)	Error in LBM(%)
(a)	7.82E-3	8.28E-3	−5.6
(b)	1.38E-2	1.43E-2	−3.5
(c)	2.17E-2	2.15E-2	+0.9
(d)	3.11E-2	3.08E-2	+1.0
(e)	5.03E-2	5.05E-2	−0.4

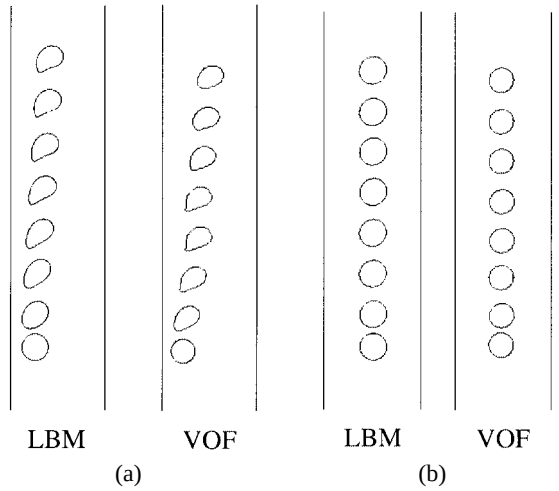

Fig. 5 The trajectories of bubble in uniform shear flow for (a) E_o=10, M=0.82, and (b) E_o=1, M=0.089, simulated by LBM and VOF method

are similar in both results for Case (a), as shown in **Fig. 6**.

Third, we simulated the two-dimensional motions of two bubbles for E_o=10 in a duct, where two stationary walls are placed 40 lattice sites away from the duct center. The fluid enters uniformly at the top boundary and leaves continuously at the bottom boundary so that the bubbles stay within the computed flow field. Initially, two circular-shaped bubbles of d_B=20 are placed three bubble diameter away from each other. **Figure 7** shows the time series of snap shots of the bubbles simulated with LBM and VOF method respectively. The time interval of the shots corresponds to 2,500 time steps in LBM. The upper bubble takes a shape of skirt as the lower one approaches due to the wake formation in both results by LBM and VOF method. In terms of the flow velocity and the dimensionless distance between bubbles shown in **Figs. 8** and **9**, these results agree with each other qualitatively.

2. Three-dimensional Motion of Bubble in LBM

Following the successful simulation of 2D bubble motion, we carried out the three-dimensional simulations of bubble smotion. First, we checked the surface tension σ in the 3D model through the simulation of stationary single bubble without gravity. The density difference Δn^* is 0.84 for

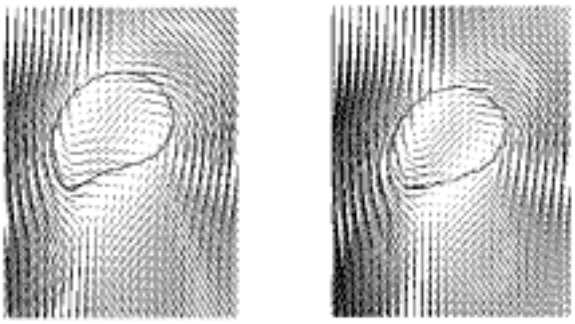

(a) LBM (b) VOF method

Fig. 6 The bubble shapes and the flow velocity fields in uniform shear flow simulated by (a) LBM and (b) VOF method for $E_o = 10$ and $M = 0.82$

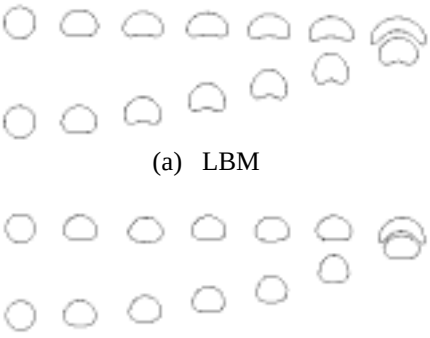

(a) LBM

(b) VOF method

Fig. 7 The time series of snap shots of bubbles for $E_o = 10$ in 2D simulations by (a) LBM and (b) VOF method

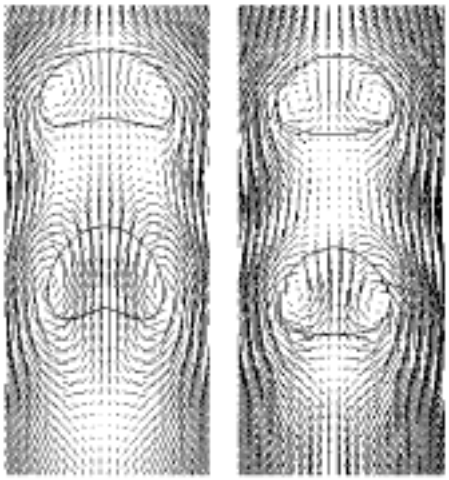

(a) LBM (b) VOF method

Fig. 8 The flow velocity fields around bubbles simulated with (a) LBM and (b) VOF method at 10,000 time steps in LBM

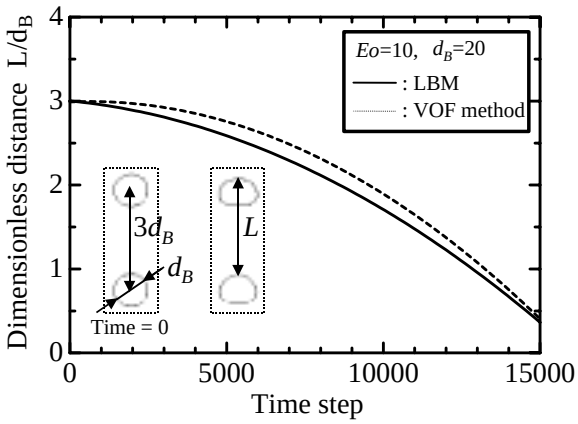

Fig. 9 The dimensionless distance between the top edges of bubbles

n_L=1.42 and n_G=0.58, corresponding to n=1, and the temperature T=0.5 is lower than critical one $T_c=\lambda/2$=0.55. In **Fig. 10**, it is shown that the pressure inside bubble with diameter d_B=20 can be controlled in this model by the parameter κ in the same way as 2D BFSY model. **Figure 11** shows the numerical results of pressure increment inside bubble with curvature of interface $1/R$ for the control parameter κ=0.01, 0.02, and 0.04. The solid lines in the figure are derived from numerical data by the least-square method in first order. The pressure difference between two phases $P_{in} - P_{out}$ increases linearly as the bubble becomes smaller, which satisfies the Laplace's law in three dimensions, $2\sigma/R = P_{in} - P_{out}$. This result also shows that the surface tension becomes larger as κ increases, such as $\sigma = 2.66\times10^{-3}$, 5.28×10^{-3}, and 8.18×10^{-3} for each κ. In addition, we simulated the coalescence of two bubbles with the diameter d_B=18 in a stationary fluid without gravity. In this case, 51^3 lattice sites are generated in the cubic space surrounded with stationary walls, and the parameters are set as follows: κ=0.01, T=0.5, n=1, Δn_0=0.495, λ=1.1, and Γ=0.1. As shown in **Fig. 12**, the spherical bubbles initially contacting to each other on their surfaces gradually fuse into a single bubble by the action of surface tension as time passes. The above results assure that the 3D surface tension is modeled properly and isotropically.

The next simulation is concerned with 3D motion of single bubble in a cylindrical tube with diameter D=35.7, where the wall is discretized with cubic lattice units to be approximately circular. In the flow field with 39^3 lattice sites, the wall is moving with the same constant velocity as terminal velocity of bubble V_t, and a liquid also inflows uniformly with V_t from upper boundary in order to simulate bubble motion in stationary liquid. The Morton and Eötvös numbers $M = 2.208\times10^{-3}$ and E_o=77.8 result from bubble diameter d_B=20.9, gas and liquid densities n_L=1.47 and n_G=0.53, kinetic viscosity ν_L=0.02, gravity $|\boldsymbol{g}|=10^{-3}$, and $\sigma = 5.28\times10^{-3}$, which is caused by κ=0.02, T=0.5 and λ=1.1 as mentioned above. The mobility Γ is 2.5. **Figure 13** shows a snap shot of bubble interface and the flow velocity field on the cross section along center line of tube. The bubble deforms to be cap-shaped and rises with $V_t = 5.24\times10^{-2}$ under the influence of wall. When $E_o \geq 40$ and M is small like this simulation, V_t can be empirically predicted from diameter ratio d_B/D and the terminal velocity in infinite media $V_{t\infty}$,[24)]

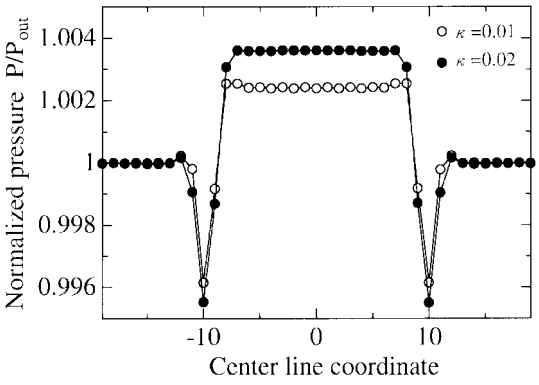

Fig. 10 The pressures inside bubble with diameter 20 for parameter κ=0.01 and 0.02

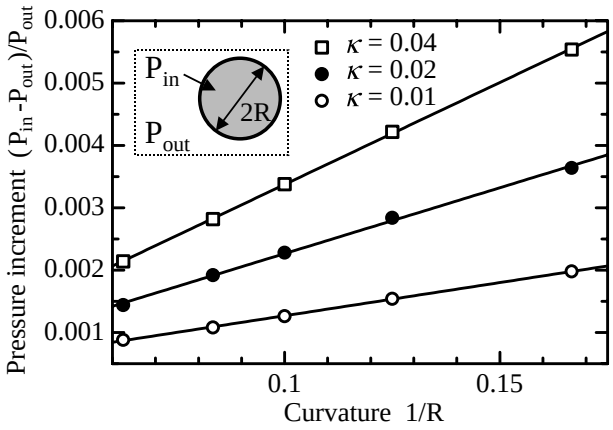

Fig. 11 The pressure increment inside bubble in 3D BFSY model for radius R and parameter κ

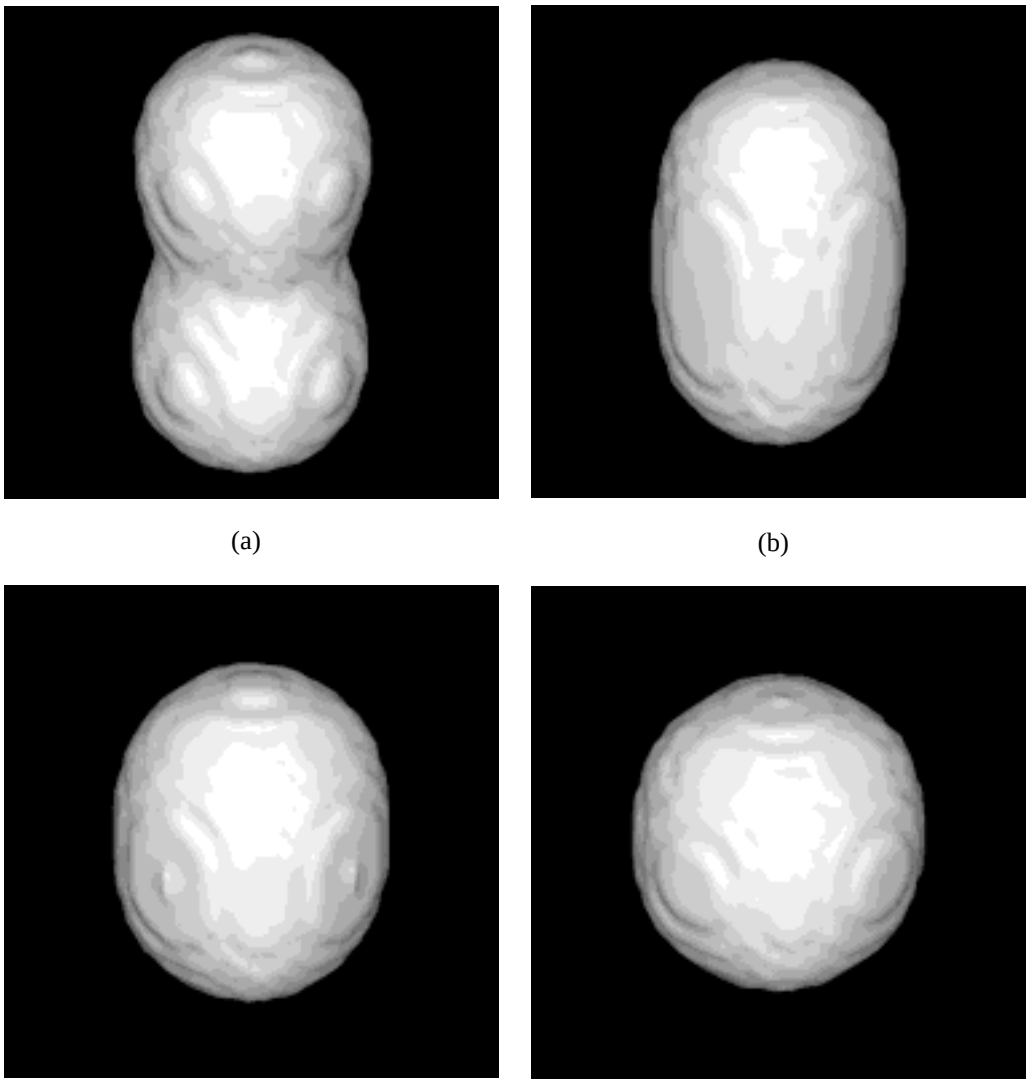

Fig. 12 The coalescence of two bubbles without gravity simulated by the 3D BFSY model at time steps: (a) 500, (b) 1,000, (c) 1,500, and (d) 2,000

$$\frac{V_t}{V_{t\infty}} = 1.13 \exp\left[-\frac{d_B}{D}\right], \tag{56}$$

where $V_{t\infty}$ is determined through a generalized graphical correlation in terms of E_o, M, and bubble Reynolds number $Re_{B\infty}=d_B V_t/\nu_L$.[25] In this case, $Re_{B\infty}$ is about 85, corresponding to $V_{t\infty}=8.13\times10^{-2}$. The ratio $V_t/V_{t\infty}=0.645$ in LBM is reasonable, compared with the prediction value 0.630 from the diameter ratio $d_B/D=0.584$.

The last simulation depicts the three-dimensional motion of two bubbles with $d_B=18$ under gravity, which are rising in the circular tube with diameter 48 in case of $E_o=50.1$, $M=1.5$ for $n=1$, $\Delta n_0=0.495$, $\kappa=0.01$, $\Gamma=0.12$, $\lambda=1.096$, $T=0.5$, and $\nu_L=0.1$. The flow field is discretized with 53, 53, and 75 lattice sites in x-, y- and z-directions respectively, and the fluid enters downward from the top boundary uniformly with the same velocity -0.022 as the tube wall. It is nearly equal to the rising velocity of bubbles and corresponds to the bubble Reynolds number $Re_b=4.0$. In the initial condition, the bubbles are initially placed away from each other by $1.4d_B$ along the center line of tube. In **Fig. 14**, the left figures show the bubble surfaces seen from bottom side, while the right figures show the bubble profile and the flow velocity on the vertical cross section through the center of tube. As seen in 2D simulation, the trailing bubble approaches the leading one due to the wake formation, and they coalesce into a single bubble eventually. The above-mentioned results suggest that 3D BFSY model is appropriately installed for the numerical simulation of bubble motions.

VI. Concluding Remarks

In the lattice Boltzmann method (LBM), we developed the three-dimensional version of the binary fluid model and introduced the buoyancy effect on the definition of Eötvös and Morton numbers in order to simulate two-phase fluid motions under gravity. Lattice Boltzmann method possesses the advantage that an interface is reproduced in a self-organizing way by introducing the repulsive interaction between mesoscopic fluid particles. From this point, we think that it can play an important role to numerically analyze multiphase fluid system.

Three kinds of two-dimensional simulation were carried out, compared with those by the Volume of Fluid (VOF) method using the Navier-Stokes equations. First, in the simulation of single bubble rising in a duct, there are agreements between the results by LBM and VOF method. The second simulation is the bubble motion in uniform shear flow, in which the bubble located near wall slides to center of duct in the both results. In the third simulation of two rising bubbles, the result by LBM agrees qualitatively with that by VOF method.

We also carried out the three-dimensional simulations by the proposed model. The surface tension was checked through two simulations without gravity, where it satisfied the Laplace's law and two bubbles fused into a spherical-shaped one. In the simulation of single bubble rising under gravity, the terminal velocity agreed reasonably with empirical prediction from the ratio of bubble diameter to tube one. The last simulation is concerned with two-bubble motion in a circular tube full with stationary fluid. In the result, they approach due to the wake formation and coalesce into a single bubble eventually.

As described above, LBM provides not only two-dimensional numerical results consistent with those by the conventional simulation method but also reproduces three-dimensional bubble motion. This study therefore proves that the 3D model and the buoyancy effect proposed here are valid in the lattice Boltzmann simulation of bubble motion under gravity. In the simulations, the density ratios of two phases are 1 : 2.45 for 2D, and 1 : 2.77 and 1 : 2.99 for 3D simulations. These values are on the same order with the density ratio 1 : 5.44 in steam-water two-phase fluid under 16 MPa. However, LBM simulation tends to be numerically unstable in case of such actual fluid flows as those in PWR. To overcome this problem, finite difference scheme for lower Morton number is under consideration now.

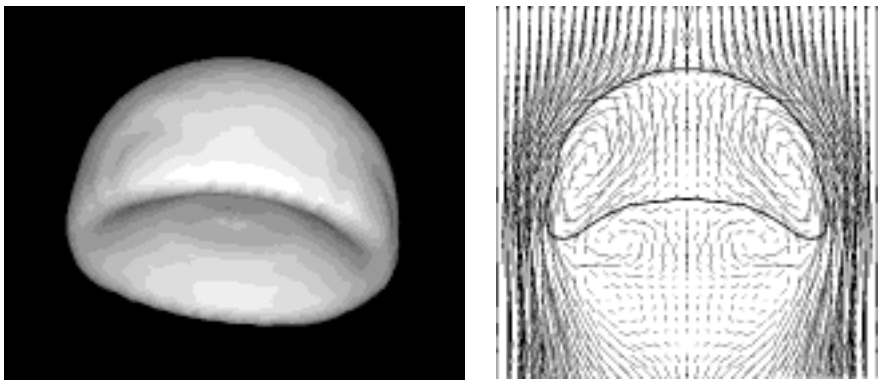

(a) Interface (b) Flow velocity

Fig. 13 The bubble rising in circular tube

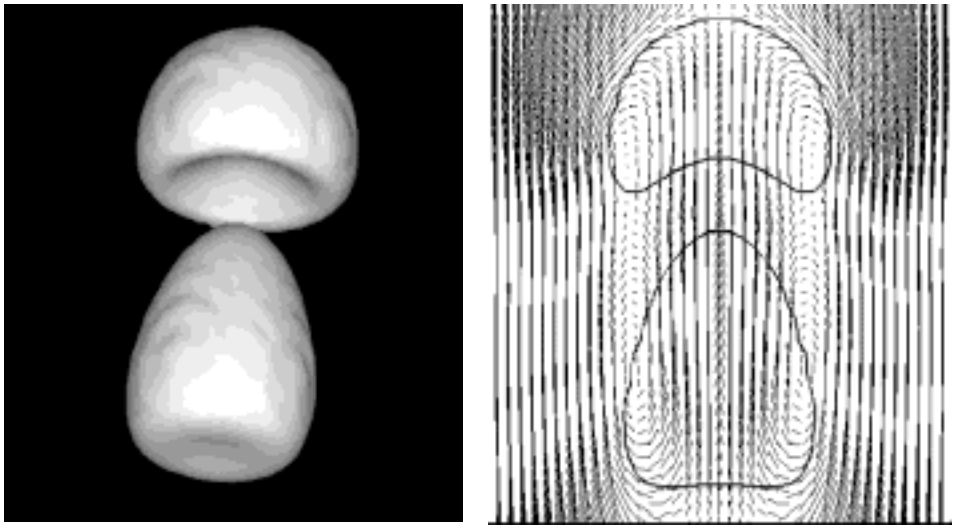

(a)

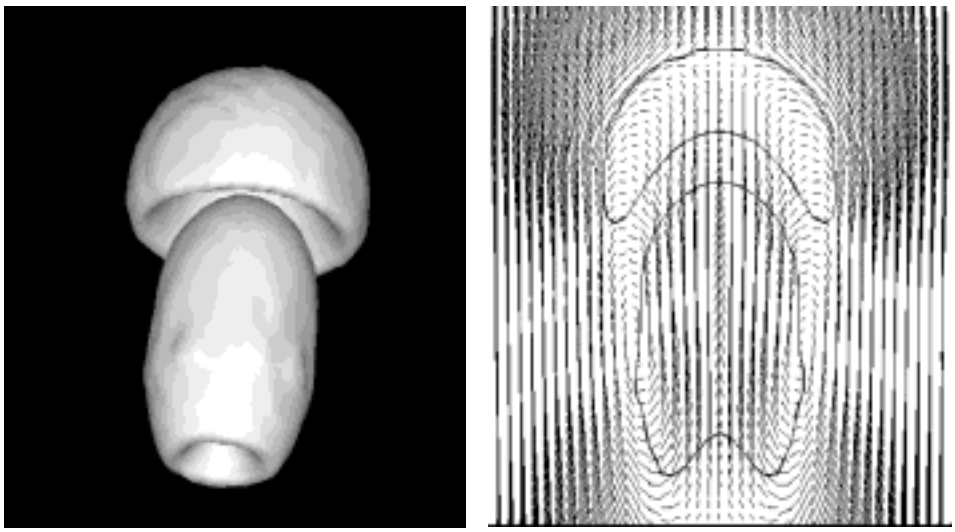

(b)

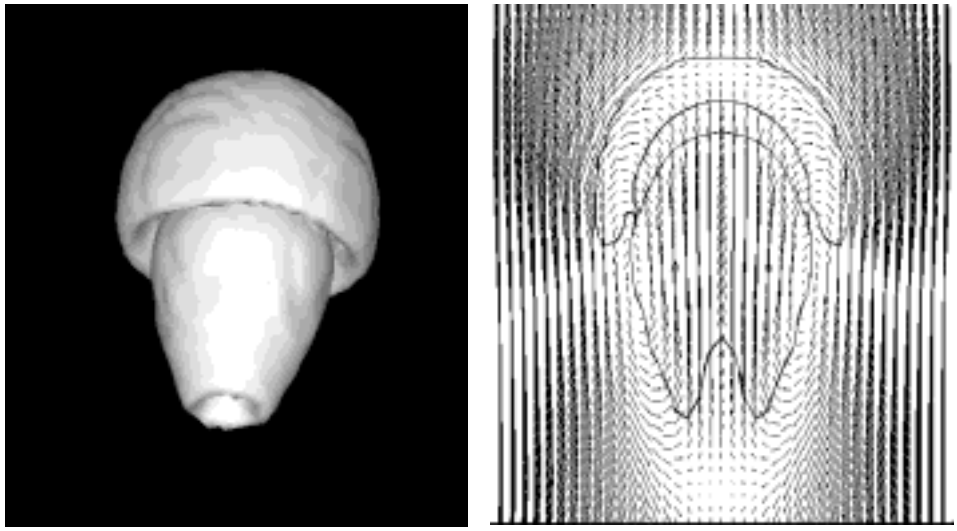

(c)

Fig. 14 (a)–(e) The 3D view of interface and the 2D flow velocity around bubbles in a circular tube at (a) 500, (b) 1,000, (c) 1,500, (d) 2,000, and (e) 2,500 time steps

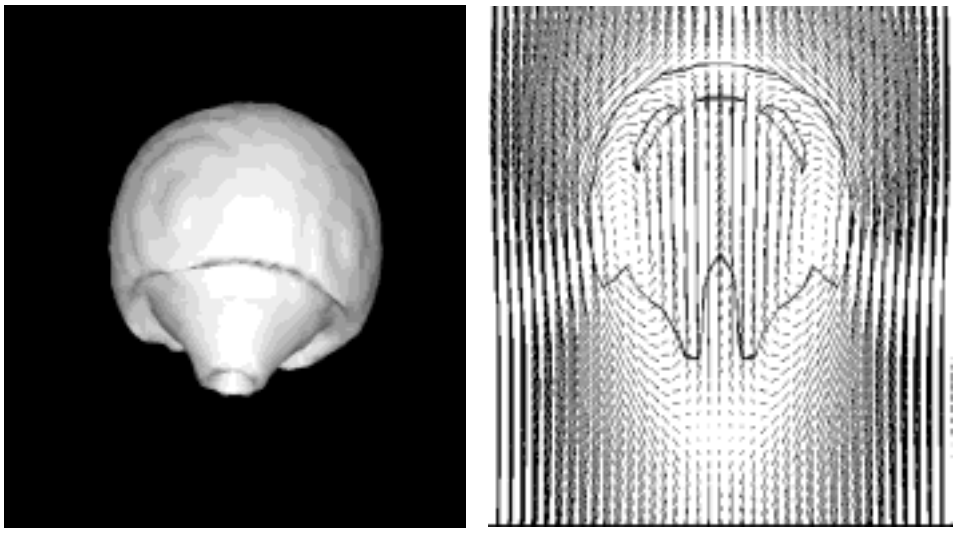

Fig. 14 (d)

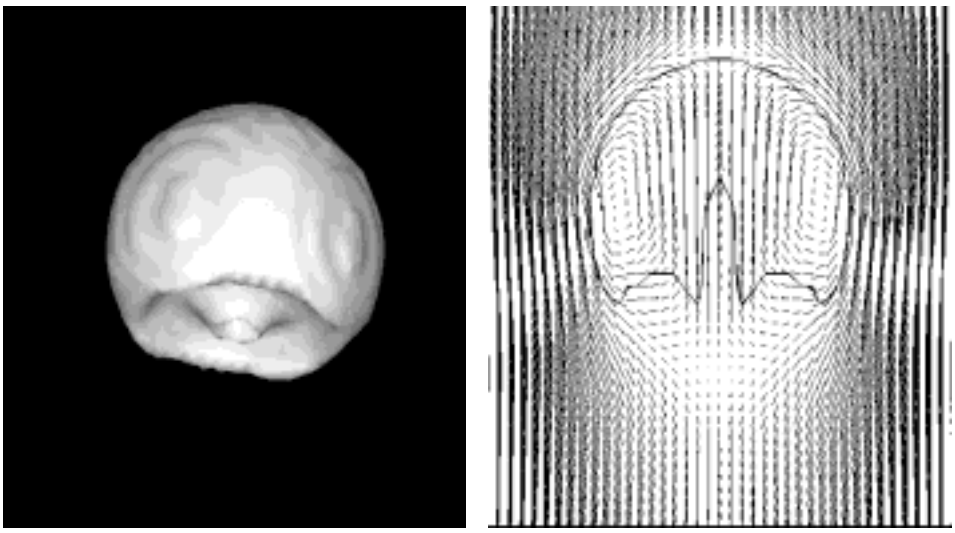

Fig. 14 (e)

References

1) G. McNamara, G. Zanetti, *Phys. Rev. Lett.*, **61**, 2332 (1988).
2) U. Frisch, *et al.*, *Phys. Rev. Lett.*, **56**, 1505 (1986).
3) U. Frisch, *et al.*, *Complex Syst.*, **1**, 649 (1987).
4) S. Hou, *et al.*, *J. Comp. Physiol.*, **118**, 329 (1994).
5) Y. Chen, *et al.*, *Phys. Rev.*, **E 50**, 2776 (1994).
6) N. Takada, M. Tsutahara, *Comp. Fluids*, **27**, 807 (1998).
7) T. Inamuro, *et al.*, *Int. J. Numer. Methods. Fluids*, **29**, 737 (1999).
8) A. K. Gunstensen, *et al.*, *Phys. Rev.*, **A 43**, 4320 (1991).
9) D. Grunau, *et al.*, *Phys. Fluids*, **A 10**, 2557 (1993).
10) X. W. Shan, H. D. Chen, *Phys. Rev.*, **E 47**, 1815 (1993).
11) X. W. Shan, H. D. Chen, *Phys. Rev.*, **E 49**, 2941 (1994).
12) M. R. Swift, *et al.*, *Phys. Rev. Lett.*, **75**, 830 (1995).
13) Y. Kato, *et al.*, *Int. J. Modern Phys.*, **C 8**, 843 (1997).
14) S. Chen, G. D. Doolen, *Annu. Rev. Fluid Mech.*, **30**, 329 (1998).
15) J. Buckles, *et al.*, *Los Alamos Sci.*, **22**, 112 (1994).
16) M. R. Swift, *et al.*, *Phys. Rev.*, **E 54**, 5041 (1996).
17) G. Gonnella, *et al.*, *Int. J. Modern Phys.*, **C 8**, 783 (1997).
18) B. T. Nadiga, S. Zaleski, *Eur. J. Mech. B/Fluids*, **15**, 885 (1996).
19) C. W. Hirt, B. D. Nichols, *J. Comp. Physiol.*, **39**, 201 (1981).
20) S. Chen, *et al.*, *J. Stat. Phys.*, **68**, 379 (1992).
21) Y. H. Qian, *et al.*, *Europhys. Lett.*, **17**, 479 (1992).
22) D. R. Noble, *et al.*, *Phys. Fluids*, **7**, 203 (1995).
23) N. Cao, *et al.*, *Phys. Rev.*, **E 55**, 21 (1997).
24) R. Crift, *et al.*, *Bubbles, Drops, and Particles*, Academic Press, California, 234 (1978).
25) J. R. Grace, *Trans. Inst. Chem. Eng.*, **51**, 116 (1973).